J Solid State Electrochem (2015) 19:569–576
DOI 10.1007/s10008-014-2635-4

ORIGINAL PAPER

Effect of particle size on rate capability and cyclic stability of $LiNi_{0.5}Mn_{1.5}O_4$ cathode for high-voltage lithium ion battery

Liang Xue · Xiaoping Li · Youhao Liao · Lidan Xing · Mengqing Xu · Weishan Li

Received: 10 May 2014 / Revised: 7 September 2014 / Accepted: 15 September 2014 / Published online: 26 September 2014

Abstract $LiNi_{0.5}Mn_{1.5}O_4$ samples with their particle sizes from micro to nano are synthesized via polyvinylpyrrolidone (PVP)-assisted coprecipitation of nickel and manganese hydroxide. Their morphology, structure, and performance as cathode of high-voltage lithium ion battery are investigated by scanning electron microscopy (SEM), X-ray diffraction (XRD), cyclic voltammetry (CV), electrochemical impedance spectroscopy (EIS), and charge/discharge test. The characterizations from SEM and XRD show that the particle size of the resulting $LiNi_{0.5}Mn_{1.5}O_4$ is tunable from micro to nano by controlling the concentrations of PVP for the formation of nickel and manganese hydroxide precursor. The results from CV, EIS, and charge/discharge test reveal that reducing the particle size of $LiNi_{0.5}Mn_{1.5}O_4$ results in its less interfacial resistance for lithium insertion/desertion process, leading to its improved rate capability. Meanwhile, the cyclic stability of $LiNi_{0.5}Mn_{1.5}O_4$ is also improved when its particle size is changed from micro to nano, but too smaller particle size is not beneficial to its cyclic stability, especially at elevated temperature. When evaluated in $LiNi_{0.5}Mn_{1.5}O_4$/Li half cell, the resulting $LiNi_{0.5}Mn_{1.5}O_4$ samples of 800, 250, and 125 nm, in average, deliver a 20 C rate capacity of 40, 58, and 71 mAh g^{-1}, while they exhibit a capacity retention of 79, 89, and 82 % after 250 cycles with 0.5 C rate at room temperature and 33, 77, and 64 % after 200 cycles with 1 C rate at 55 °C, respectively. This difference in capacity retention becomes more significant in $LiNi_{0.5}Mn_{1.5}O_4$/graphite full cells due to the effect of graphite anode.

Keywords Lithium nickel manganese oxide · Particle size · Rate capability · Cyclic stability · High-voltage lithium ion battery

L. Xue · X. Li · Y. Liao (✉) · L. Xing · M. Xu · W. Li (✉)
School of Chemistry and Environment, Key Laboratory of Electrochemical Technology on Energy Storage and Power Generation of Guangdong Higher Education Institutes, and Engineering Research Center of Materials and Technology for Electrochemical Energy Storage (Ministry of Education), South China Normal University, Guangzhou 510006, China
e-mail: liaoyouhao@126.com
e-mail: liwsh@scnu.edu.cn

Y. Liao
Guangdong Zhongke Xintai New Energy Co. Ltd., Jieyang 515559, China

Introduction

Compared with other energy storage devices, lithium ion battery has attracted much attention because it delivers higher energy density and exhibits better cycle performance [1, 2]. Furthermore, the energy density of lithium ion battery can be improved by substituting new cathode and anode materials for currently used cobalt-based cathode and graphite anode. $LiNi_{0.5}Mn_{1.5}O_4$ is considered as a promising cathode material for improving the high energy density of lithium ion battery due to its high operating voltage of 4.7 V (*vs.* Li/Li^+) [3–5]. However, the rate capability and cyclic stability of $LiNi_{0.5}Mn_{1.5}O_4$ need to be improved. $LiNi_{0.5}Mn_{1.5}O_4$ exhibits poor electronic conductivity, leading to poor rate capability [6, 7]. The manganese dissolution and the particle separation might happen during charge and discharge cycling, resulting in the deteriorated cyclic stability of $LiNi_{0.5}Mn_{1.5}O_4$ [5, 8, 9].

Many investigations have been focused on fabricating nanoparticles to improve rate capability and cyclic stability of $LiNi_{0.5}Mn_{1.5}O_4$ [10–19]. Nanoparticles provide short paths for lithium ion transportation in particles and large interface between nanoparticles and electrolyte for lithium insertion/desertion, thus enhancing the rate capability of $LiNi_{0.5}Mn_{1.5}O_4$. On the other hand, the space among nanoparticles accommodates the lattice stress caused by Jahn-Teller distortion during cycles and avoids the particle separation, thus improving the cyclic stability of $LiNi_{0.5}Mn_{1.5}O_4$ [12].

The large interface that nanoparticles provide increases sites for lithium insertion/desertion reaction between cathode materials and electrolyte and facilitates rate capability improvement. However, the increased sites for lithium insertion/desertion reaction also increase the possibility of the decomposition of cathode materials and electrolyte, leading to a capacity decaying and a deteriorated cyclic stability [20–22], especially in $LiNi_{0.5}Mn_{1.5}O_4$/graphite full cell [23]. Therefore, an issue remains in the synthesis and application of $LiNi_{0.5}Mn_{1.5}O_4$: What particle size is suitable for the improvement in rate capability as well as cyclic stability of $LiNi_{0.5}Mn_{1.5}O_4$?

To answer this question, $LiNi_{0.5}Mn_{1.5}O_4$ samples with their particle sizes from micro to nano were synthesized, and the effect of particle size on the rate capability and cyclic stability of $LiNi_{0.5}Mn_{1.5}O_4$ as cathode of high-voltage lithium ion battery was understood in this paper. To our knowledge, it is the first time to consider simultaneously the contribution of the particle size to rate capability and cyclic stability of $LiNi_{0.5}Mn_{1.5}O_4$. The particle size of $LiNi_{0.5}Mn_{1.5}O_4$ was controlled by using polyvinylpyrrolidone (PVP) to limit the particle size of nickel manganese hydroxide precursor [12, 24, 25]. The prepared samples were assembled into $LiNi_{0.5}Mn_{1.5}O_4$/Li half cells and $LiNi_{0.5}Mn_{1.5}O_4$/graphite full cells, and charge-discharge tests were performed at room and elevated temperature to verify the effect of particle size.

Experimental

Sample preparation

Three $LiNi_{0.5}Mn_{1.5}O_4$ samples were synthesized by PVP-assisted coprecipitation and subsequent solid reaction. PVP with 0, 0.5, and 1 g was dispersed in 50 mL distilled water, respectively. Subsequently, nickel acetate ($Ni(CH_3COO)_2{\cdot}4H_2O$) and manganese acetate ($Mn(CH_3COO)_2{\cdot}4H_2O$) were added in a stoichiometric amount. One-molar lithium hydroxide (LiOH) aqueous solution was added slowly under continuous stirring at 80 °C to disperse PVP uniformly. The reaction time for the formation of transition metal hydroxide ($Ni_{0.5}Mn_{1.5}(OH)_4$) was 24 h. The precipitate was washed, filtrated, and dried in oven 120 °C for 12 h, and three precursors were obtained, denoted as NMO-A, NMO-B, and NMO-C from 0, 0.5, and 1 g PVP, respectively.

$Ni_{0.5}Mn_{1.5}(OH)_4$ precursor was mixed uniformly with lithium hydroxide in a stoichiometric ratio by ball-grinding. The mixture was calcined at 500 °C for 0.5 h and then at 800 °C for 8 h. Three $LiNi_{0.5}Mn_{1.5}O_4$ products were obtained, denoted as LMNO-A, LMNO-B, and LMNO-C from NMO-A, NMO-B, and NMO-C, respectively.

Physical characterization

The morphology was observed using scanning electron microscopy (SEM, JEOL JSM-6380LA, Japan). The crystal structure was characterized by powder X-ray diffraction (XRD, Bruker D8 AdVANCE, Germany) with Cu-Ka radiation (40 kV, 40 mA) from 10° to 80° with a step of 0.02°.

Electrochemical measurements

The electrode was prepared by mixing 80 wt% of prepared sample, 10 wt% of carbon black, and 10 wt% of polyvinylidene difluoride (PVDF) as a binder, coating the mixture onto an aluminum sheet, which was dried at 80 °C in an oven and cut into pieces of 1 cm×1 cm. The coin cells (CR2025) were assembled in an argon-filled glove box (MBraun) by using the prepared electrode as cathode, lithium foil or graphite electrode as anode, Celgard 2400 as separator, and 1 M $LiPF_6$ in EC/DMC (1:2 in volume) as electrolyte. The cyclic voltammetry was performed with Solartron-1470E Cell-test at 25 °C between 3.0 and 5.0 V with a scanning rate of 0.2 mV s^{-1}. Electrochemical impedance measurements were carried out on Autolab (PGSTAT302N) in the frequency range between 100 kHz and 0.01 Hz, and the perturbation amplitude was controlled at 10 mV. Charge-discharge tests were performed on Multi-channel Battery Testers (LAND CT2001A, China) with various rates from 0.5 to 20 C between 3.0 and 5.0 V.

Results and discussion

Crystal structure and morphology

The observed morphology of the resulting precursors and products is presented in Fig. 1. It can be seen from Fig. 1a1, b1, c1 that the concentration of PVP affects significantly the morphology of the precursors. Without using PVP, the resulting precursor (NMO-A) is bulky, as shown in Fig. 1a1. With using PVP, however, the uniformly dispersed nanoparticles of the precursors (NMO-B and NMO-C) can be identified in Fig. 1b1, c1. The particle size of the precursor decreases with increasing the concentration of PVP. It is obvious that PVP functions as a particle controller for the formation of the precursor. The morphology of the precursors subsequently affects that of $LiNi_{0.5}Mn_{1.5}O_4$ products, as shown in Fig. 1a2, b2, c2.

Figure 2 presents the particle size distribution of $LiNi_{0.5}Mn_{1.5}O_4$ products. The particles are large (800 nm in average) and distributed irregularly for product LNMO-A, as shown in Figs. 1a2 and 2a, while they become smaller and distributed uniformly for the products LNMO-B and LNMO-C, as shown in Figs. 1b2, c2 and 2b, c. Due to the difference of

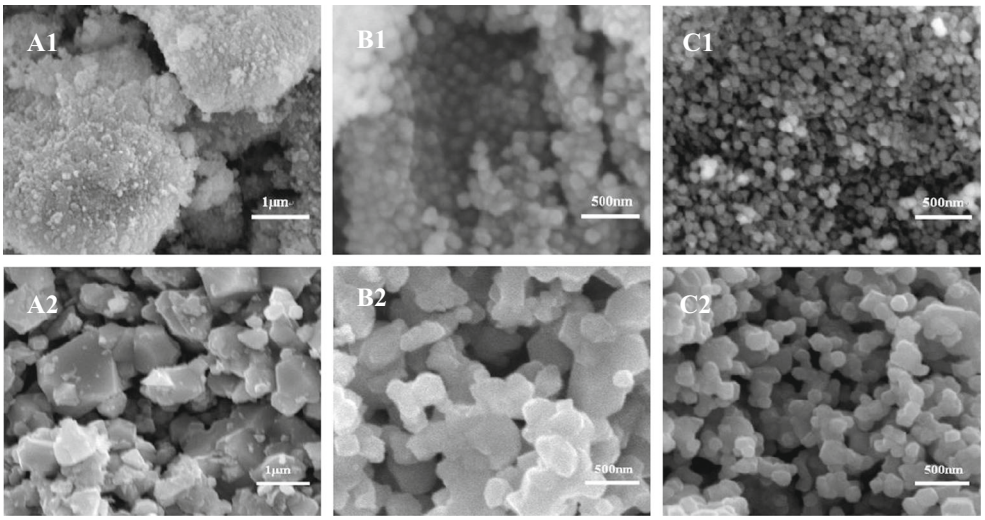

Fig. 1 SEM images of metal hydroxide precursors, MNO-A (**a1**), MNO-B (**b1**), and MNO-C (**c1**), and $LiNi_{0.5}Mn_{1.5}O_4$ products, LNMO-A (**a2**), LNMO-B (**b2**), and LNMO-C (**c2**)

their precursors, LNMO-B and LMNO-C have their average particle sizes of 250 and 125 nm, respectively.

The formation process of $LiNi_{0.5}Mn_{1.5}O_4$ is illustrated in Scheme 1. PVP restricts the growth space of particles during the coprecipitation process of the nickel and manganese oxide [26]. The larger the concentration of PVP is, the smaller the space available for the formation of the precursor is. The morphology of the resulting $LiNi_{0.5}Mn_{1.5}O_4$ is tightly related to its precursor. It can be seen from Figs. 1 and 2 that the particle size of $LiNi_{0.5}Mn_{1.5}O_4$ is tunable from micro to nano by controlling the concentration of PVP for the formation of $Ni_{0.5}Mn_{1.5}(OH)_4$ precursor.

The crystal structure of the resulting products was determined by XRD. Figure 3 presents the XRD patterns of LNMO-A, LNMO-B, and LNMO-C. Compared with the standard card of $LiNi_{0.5}Mn_{1.5}O_4$ (JCPD# 80–2162), it can be found that three products are well-defined cubic spinels with the space group Fd-3 m and do not contain any impurity phase. The lattice constant obtained by Rietveld refinement from XRD data is 8.169 Å for LNMO-A, 8.170 Å for LNMO-B, and 8.169 Å for LNMO-C. Three samples have almost the

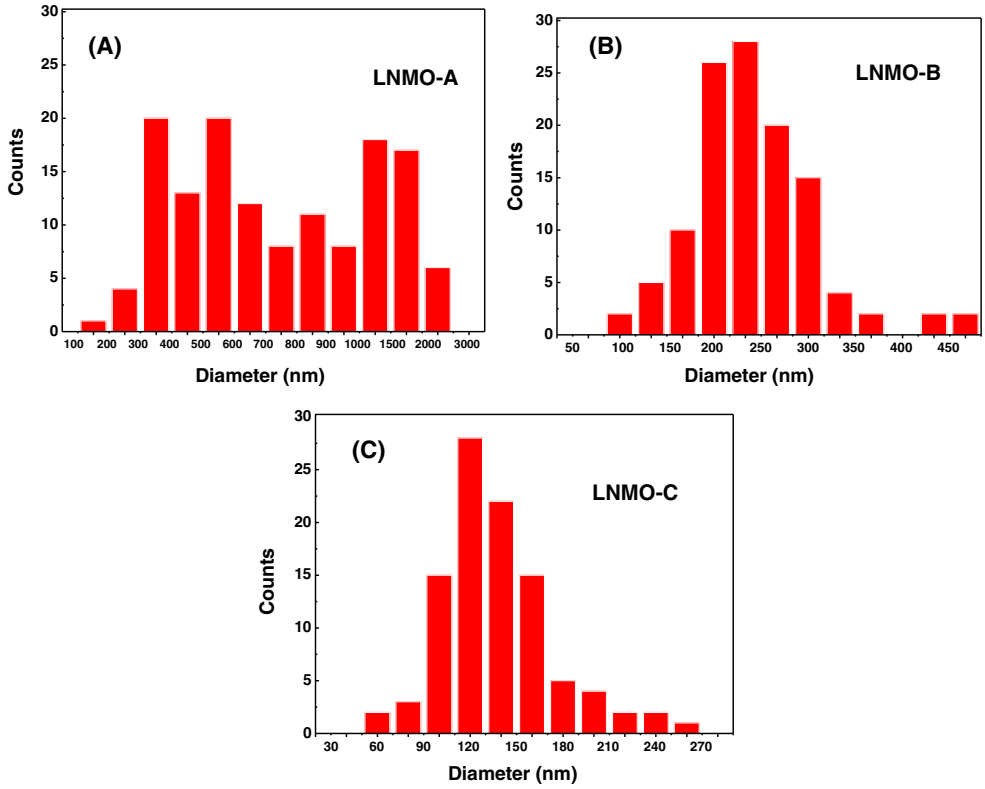

Fig. 2 Particle size distribution of $LiNi_{0.5}M_{1.5}O_4$ samples

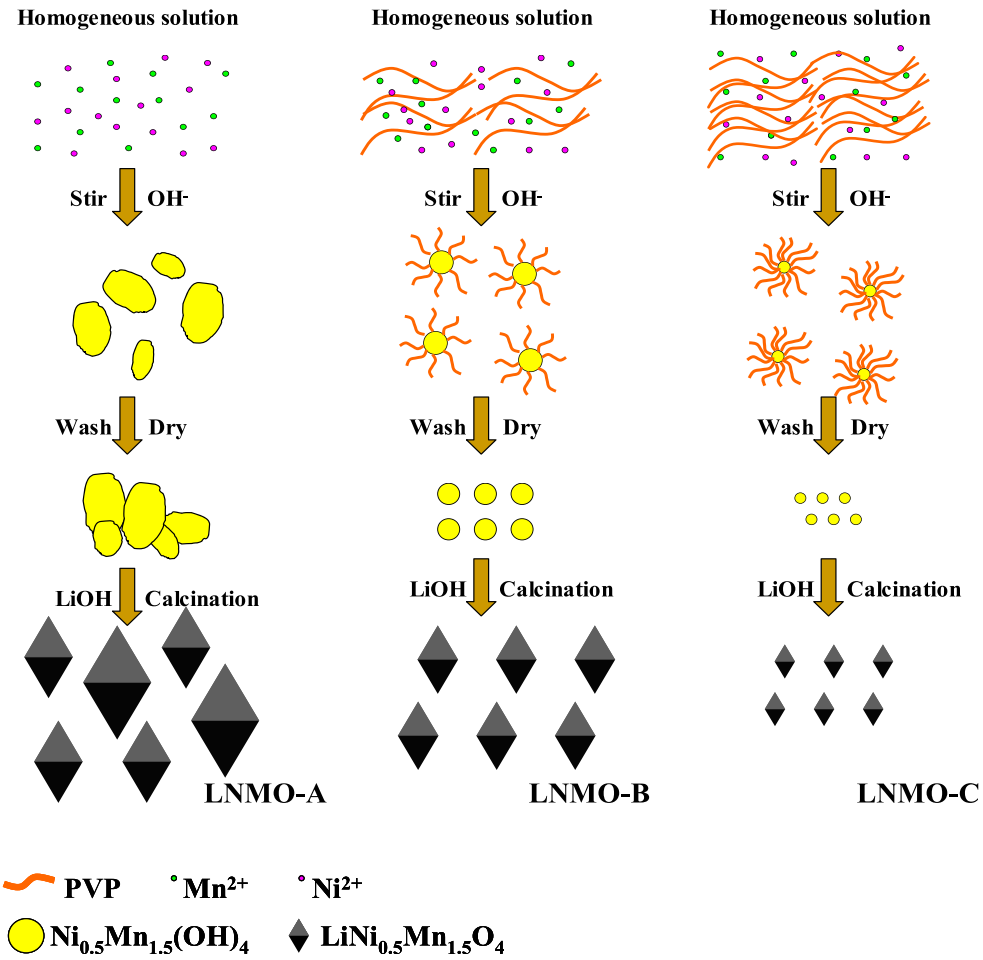

Scheme 1 Schematic formation process of $LiNi_{0.5}Mn_{1.5}O_4$ products

same lattice constant, indicating that PVP controls the particle size but does not change the crystal structure of the resulting $LiNi_{0.5}Mn_{1.5}O_4$.

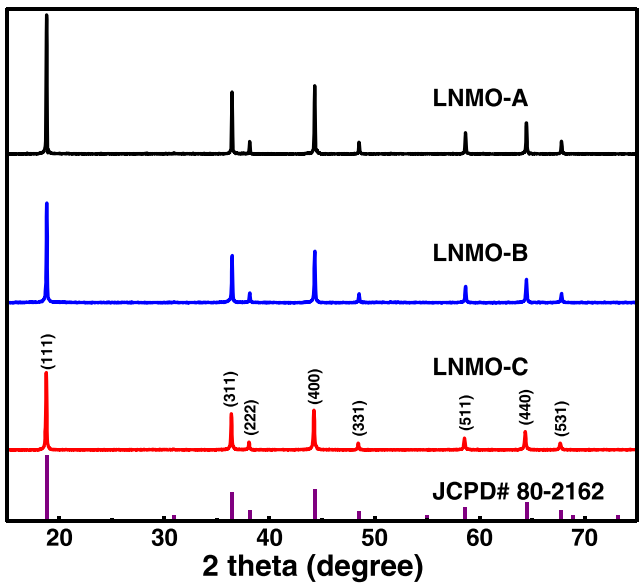

Fig. 3 XRD patterns of $LiNi_{0.5}Mn_{1.5}O_4$ products and the standard card of spinel $LiNi_{0.5}Mn_{1.5}O_4$

Electrochemical performances

The reversibility of the three $LiNi_{0.5}Mn_{1.5}O_4$ samples for lithium insertion/desertion was understood by cyclic voltammetry. Figure 4 shows the cyclic voltammograms of

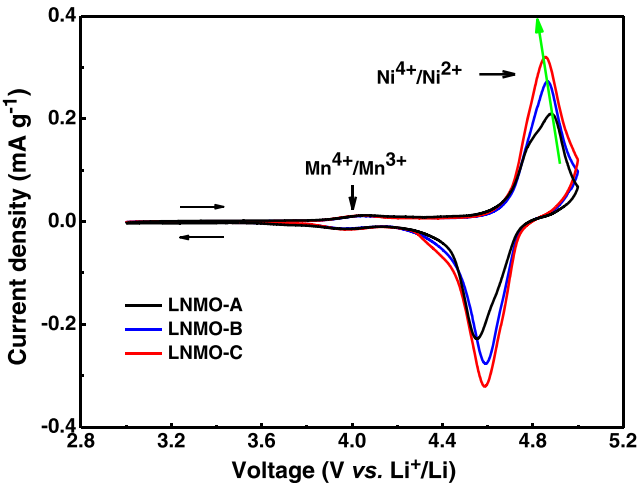

Fig. 4 Cyclic voltammograms of $LiNi_{0.5}Mn_{1.5}O_4$ electrodes at a scan rate of 0.2 mV s^{-1}

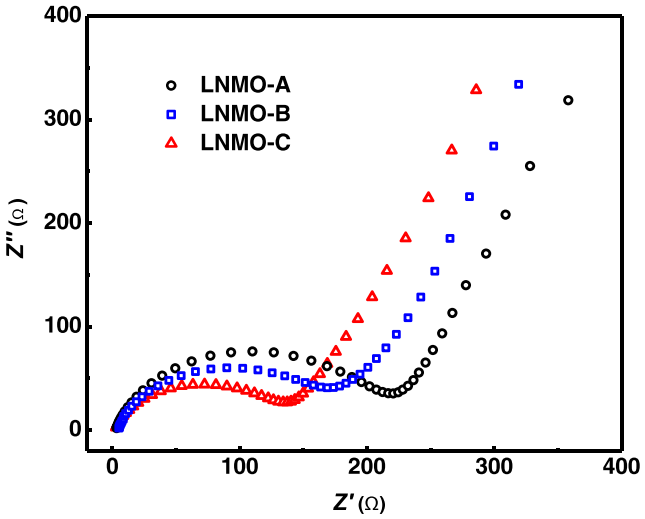

Fig. 5 Electrochemical impedance spectra of $LiNi_{0.5}Mn_{1.5}O_4$ electrodes, measured at 3.0 V after 10 cycles of cyclic voltammetry with a scan rate of 0.2 mV s^{-1} between 3.0 and 5.0 V

LNMO-A, LNMO-B, and LNMO-C at a scanning rate of 0.2 mV s^{-1} between 3.0 and 5.0 V. Two couple of redox peaks can be clearly identified at about 4.0 V corresponding to Mn^{4+}/Mn^{3+} reaction and about 4.7 V corresponding to Ni^{4+}/Ni^{2+} reaction, which are the characteristics of $LiNi_{0.5}Mn_{1.5}O_4$ with Fd-3 m space group. The Ni^{4+}/Ni^{2+} reaction contributes mainly to lithium insertion/desertion capacity of $LiNi_{0.5}Mn_{1.5}O_4$. It can be found from Fig. 4 that the potential difference of Ni^{4+}/Ni^{2+} reaction decreases in the order of LNMO-A, LNMO-B, and LNMO-C, indicating that LNMO-C has the best reversibility for lithium insertion/desertion, followed by LNMO-B and then LNMO-A. That is to say, particle size of $LiNi_{0.5}Mn_{1.5}O_4$ affects the reversibility or polarization of lithium insertion/desertion process. Reducing particle size increases the reversibility or decreases the polarization of lithium insertion/desertion process.

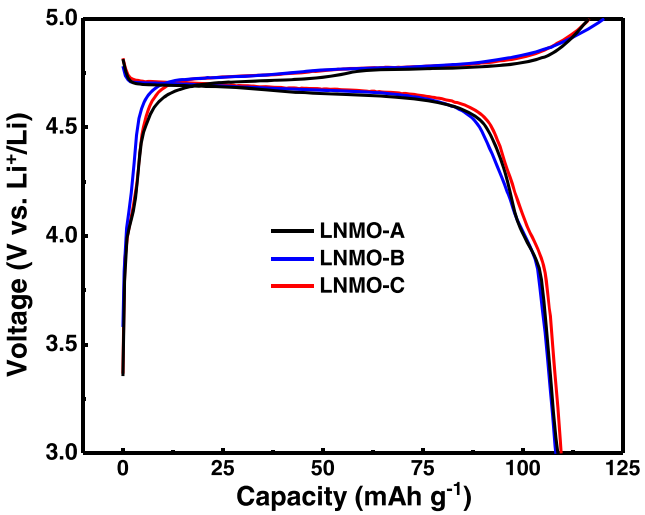

Fig. 6 Charge/discharge curves of $LiNi_{0.5}Mn_{1.5}O_4$ electrodes at 0.5 C rate between 3.0 and 5.0 V

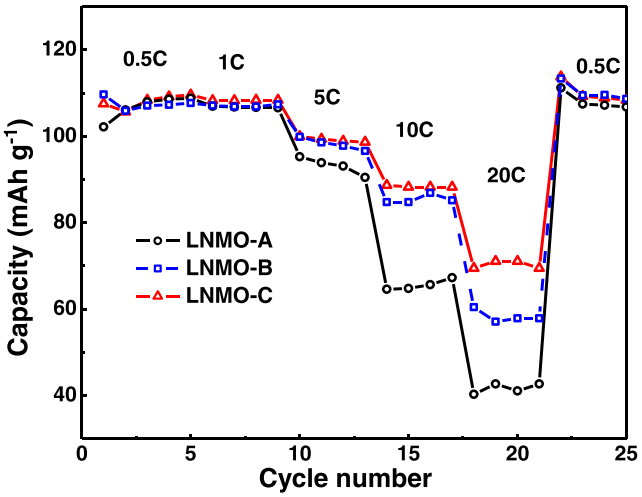

Fig. 7 Rate capability of $LiNi_{0.5}Mn_{1.5}O_4$ electrodes cycled between 3.0 and 5.0 V

The improved reversibility of lithium insertion/desertion in $LiNi_{0.5}Mn_{1.5}O_4$ by reducing particle size was confirmed with EIS. Figure 5 presents the electrochemical impedance spectra of LNMO-A, LNMO-B, and LNMO-C after 10 cycles of CV, which are characteristic of a semicircle at high frequencies and a slope line at low frequencies. The semicircle reflects the interfacial properties between cathode materials and electrolyte, while the slope line represents the diffusion of lithium ion in cathode. The reaction resistance for lithium insertion/desertion can be estimated by the diameter of the semicircle. It is 225 Ω for LNMO-A, 115 Ω for LNMO-B, and 108 Ω for LNMO-C, which is the same order as the potential difference in CV measurement. The decreased reaction resistance is important for the rate capability improvement of $LiNi_{0.5}Mn_{1.5}O_4$ as cathode of lithium ion battery.

Figure 6 presents the charge/discharge curves of LNMO-A, LNMO-B, and LNMO-C at 0.5 C rate between 3.0 and 5.0 V. The short potential plateau at about 4.0 V is attributed to

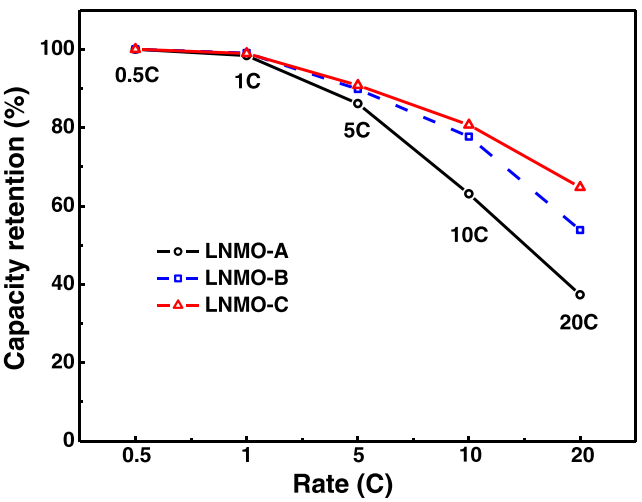

Fig. 8 Dependence of discharge capacity retention of $LiNi_{0.5}Mn_{1.5}O_4$ electrodes on the different discharged rates

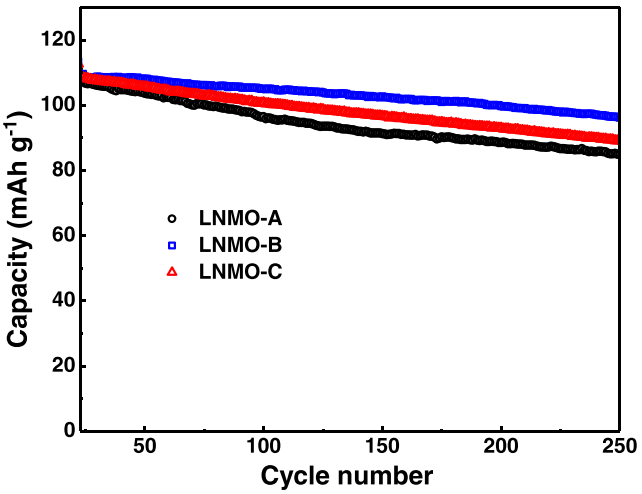

Fig. 9 Cyclic stability of $LiNi_{0.5}Mn_{1.5}O_4$ electrodes with 0.5 C rate at room temperature

Mn^{4+}/Mn^{3+} redox reaction, while the main capacity at about 4.7 V plateau is ascribed to Ni^{4+}/Ni^{2+} redox reactions [27, 28]. Three samples exhibit similar charge/discharge behavior and deliver similar discharge capacity at 0.5 C. When increasing the current rate, however, the significant difference in discharge capacity among three samples can be observed.

Figure 7 presents the rate performance of LNMO-A, LNMO-B, and LNMO-C, which was obtained in $LiNi_{0.5}Mn_{1.5}O_4$/Li half cells charged to 5 V at 0.5 C (1 C= 147 mA g^{-1}) and discharged to 3 V at different rates. Three samples deliver a similar discharge capacity of about 110 mAh g^{-1} at 0.5 C, but the average discharge capacity decreases when increasing discharge rates, which is similar to the samples doped with cobalt and chromium [29]. LNMO-A has the fast capacity decrease, followed by LNMO-B, while LNMO-C delivers the highest discharge capacity under the same discharge rate. At 20 C, the average discharge capacity is 40 mAh g^{-1} for LNMO-A, 58 mAh g^{-1} for LNMO-B, and 71 mAh g^{-1} for LNMO-C. Figure 8 presents the discharge capacity retention of three samples at different rates compared to their 0.5 C discharge capacity, which show obviously the effect of $LiNi_{0.5}Mn_{1.5}O_4$ particle size on its rate capability: The rate capability of $LiNi_{0.5}Mn_{1.5}O_4$ is improved significantly by reducing its particle size. Reducing particle size decreases the lithium diffusion distance in $LiNi_{0.5}Mn_{1.5}O_4$ particle and increases the contact area between $LiNi_{0.5}Mn_{1.5}O_4$ and electrolyte, leading to the decreased reaction resistance or polarization for lithium insertion/desertion in $LiNi_{0.5}Mn_{1.5}O_4$ and thus improving the rate capability of $LiNi_{0.5}Mn_{1.5}O_4$ [13, 30, 31].

It can be noted from Fig. 7 that the initial 0.5 C discharge capacity of three samples can be recovered after the rate test. This suggests that the interface between $LiNi_{0.5}Mn_{1.5}O_4$ and electrolyte remains stable, i.e., no significant decompositions of $LiNi_{0.5}Mn_{1.5}O_4$ and electrolyte happen during the rate test. When deep cycling was

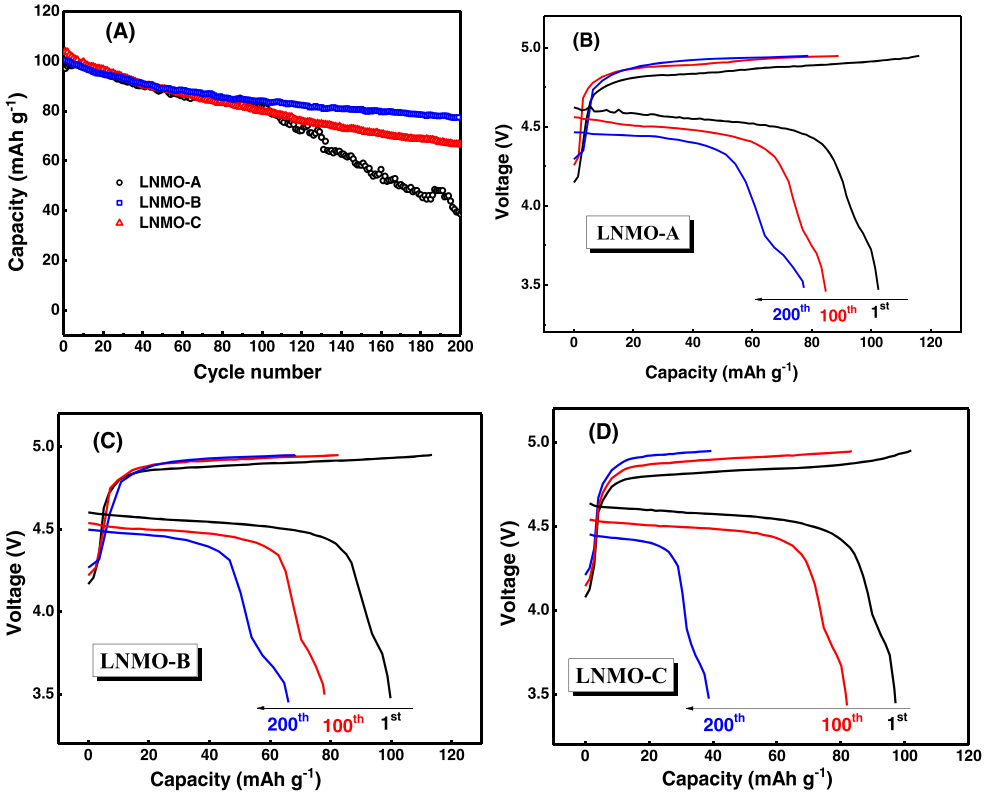

Fig. 10 Cyclic stability (**a**) and charge/discharge curves (**b**, **c**, **d**) of $LiNi_{0.5}Mn_{1.5}O_4$ electrodes with 1 C rate at 50 °C

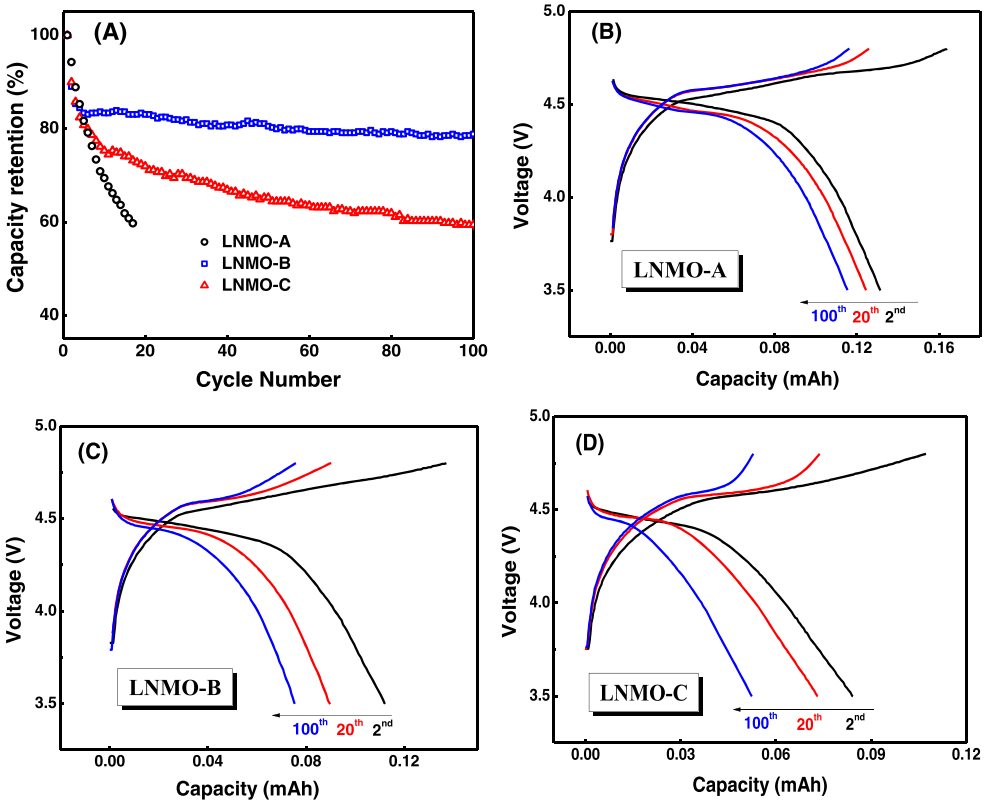

Fig. 11 Cyclic stability (**a**) and charge/discharge curves (**b**, **c**, **d**) of LNMO/graphite cells with 0.5 C rate at room temperature

performed, however, different capacity decaying was observed among three samples.

Figure 9 presents the cyclic stability of three samples under 0.5 C rate. The test was performed after rate test at room temperature. It can be seen from Fig. 9 that both LNMO-B and LNMO-C exhibits better cyclic stability than LNMO-A, while LNMO-C is poorer than LNMO-B. After 250 cycles, the capacity retention is 79 % for LNMO-A, 89 % for LNMO-B, and 82 % for LNMO-C. This result suggests that the cyclic stability of $LiNi_{0.5}Mn_{1.5}O_4$ can be also improved by changing particle size from micro to nano, but too smaller particle size will deteriorate its cyclic stability.

This phenomenon was observed more obviously when the cycling was performed at elevated temperature. Figure 10a presents the cyclic stability of three samples with 1 C rate at 50 °C, and the detail charging/discharging curves are exhibited in Fig. 10b, c, d. Similarly to the results of Fig. 9, both LNMO-B and LNMO-C exhibit better cyclic stability than LNMO-A, and LNMO-C is poorer than LNMO-B, but the difference in capacity retention becomes more significantly among three samples. The capacity retention is 33 % for LNMO-A, 77 % for LNMO-B, and 64 % for LNMO-C after 200 cycles.

LNMO-B and LNMO-C have smaller and more uniformly distributed particles, which provide more space to release the stress resulting from Jahn-Teller distortion and to avoid the destruction of $LiNi_{0.5}Mn_{1.5}O_4$ particles than LNMO-A, and thus exhibit not only better rate capability but also better cyclic stability than LNMO-A [32]. On the other hand, the smaller particle size of LNMO-C than LNMO-B increases the possibility of the decompositions of $LiNi_{0.5}Mn_{1.5}O_4$ and electrolyte due to the increased contact areas, resulting in the poorer cyclic stability of LNMO-C than LNMO-B. Therefore, suitable particle size is required to achieve the best performance of $LiNi_{0.5}Mn_{1.5}O_4$ in terms of rate capability and cyclic stability. Our results demonstrate that $LiNi_{0.5}Mn_{1.5}O_4$ with its particle size limited between micro and nano exhibits simultaneously the best rate capability and cyclic stability.

The dissolved manganese from cathode transports to anode and deposits on lithium anode in $LiNi_{0.5}Mn_{1.5}O_4$/Li half cells. In $LiNi_{0.5}Mn_{1.5}O_4$/graphite full cells, the deposited manganese accelerates the electrolyte decomposition on graphite, which is detrimental for the formation of protective solid electrolyte interphase film on graphite, resulting in faster capacity decay of the full cell than half cell [23, 33]. The cyclic stability of $LiNi_{0.5}Mn_{1.5}O_4$ samples was also evaluated in $LiNi_{0.5}Mn_{1.5}O_4$/graphite full cells; the obtained results are presented in Fig. 11. The full cells were charged at 0.5 C to 4.8 V and discharged at the same rate to 3.5 V at room temperature. Figure 11a

presents the cyclic performance, while Fig. 11b, c, d presents the charge-discharge profiles. It can be found by comparing Fig. 11a with Fig. 9 that the samples suffer more serious capacity decaying in the full cell. For example, LNMO-A delivers less than 60 % of its initial capacity after 20 cycles. As shown in Fig. 11a. LNMO-B also exhibits better cyclic stability than LNMO-C. The capacity retention is 78.8 % for LNMO-B, while only 59.0 % for LNMO-C. This result confirms that the effect of particle size of $LiNi_{0.5}Mn_{1.5}O_4$ on its cyclic stability becomes more significant in the full cell than in the half cell.

Conclusions

$LiNi_{0.5}Mn_{1.5}O_4$ with its particle size being tunable from micro to nano can be synthesized via the coprecipitation of nickel and manganese hydroxide with PVP as particle controller. The PVP facilitates the formation of the hydroxide with uniformly dispersed particles and thus control the particle size but does not change the crystal structure of the resulting $LiNi_{0.5}Mn_{1.5}O_4$. $LiNi_{0.5}Mn_{1.5}O_4$ with smaller particle size has less resistance or less polarization for lithium insertion/desertion process, and thus exhibits better rate capability. On the other hand, the cyclic stability of $LiNi_{0.5}Mn_{1.5}O_4$ is also improved when its particle size is changed from micro to nano, because the more space is available among the smaller particles to release the stress resulting from Jahn-Teller distortion and to avoid the destruction of $LiNi_{0.5}Mn_{1.5}O_4$ particles. However, too smaller particle size is not beneficial to the cyclic stability of $LiNi_{0.5}Mn_{1.5}O_4$, especially at elevated temperature and in $LiNi_{0.5}Mn_{1.5}O_4$/graphite full cells, because the decompositions of $LiNi_{0.5}Mn_{1.5}O_4$ and electrolyte due to the increased contact areas dominate the cyclic stability of $LiNi_{0.5}Mn_{1.5}O_4$.

Acknowledgments This work is financially supported from the joint project of National Natural Science Foundation of China and Natural Science Foundation of Guangdong Province (Grant No. U1134002), the National Natural Science Foundation (Grant No. 21273084), the Natural Science Fund of Guangdong Province (Grant No. 10351063101000001), the key project of Science and Technology in Guangdong Province (Grant No. 2012A010702003), Joint Project of Guangdong Province and Ministry of Education for the Cooperation among Industries, Universities and Institutes (Grant No. 2012B091100332), and the scientific research project of Department of Education of Guangdong Province (Grant No. 2013CXZDA013).

References

1. Tang W, Tian S, Liu LL, Li L, Zhang HP, Yue YB, Bai Y, Wu YP, Zhu K (2011) Electrochem Commun 13:205–208
2. Park OK, Cho Y, Lee S, Yoo HC, Song HK, Cho J (2011) Energy Environ Sci 4:1621–1633
3. Kraytsberg A, Ein-Eli Y (2012) Adv Energy Mater 2:922–939
4. Wang HL, Xia H, Lai MO, Lu L (2009) Electrochem Commun 11: 1539–1542
5. Li BZ, Xing LD, Xu MQ, Lin HB, Li WS (2013) Electrochem Commun 34:48–51
6. Fang HS, Li LP, Li GS (2007) J Power Sources 167:223–227
7. Kunduraci M, Amatucci GG (2008) Electrochim Acta 53:4193–4199
8. Ma LW, Chen BZ, Shi XC, Zhang W, Zhang K (2010) Colloids Surf A 369:88–94
9. Yoon T, Park S, Mun J, Ryu JH, Choi W, Kang YS, Park JH, Oh SM (2012) J Power Sources 215:312–316
10. Zhou L, Zhao D, Lou X (2012) Angew Chem Int Ed Engl 51:239–241
11. Zhang X, Cheng F, Yang J, Chen J (2013) Nano Lett 13:2822–2825
12. Lin HB, Zhang YM, Hu JN, Wang YT, Xing LD, Xu MQ, Li XP, Li WS (2014) J Power Sources 257:37–44
13. Shaju KM, Bruce PG (2008) Dalton Trans 5471–5475
14. Zhang X, Cheng F, Zhang K, Liang Y, Yang S, Liang J, Chen J (2012) RSC Adv 2:5669–5675
15. Rho YH, Dokko K, Kanamura K (2006) J Power Sources 157:471–476
16. Kim DK, Muralidharan P, Lee HW, Ruffo R, Yang Y, Chan CK, Peng H, Huggins RA, Cui Y (2008) Nano Lett 8:3948–3952
17. Ding YL, Goh BM, Zhang H, Loh KP, Lu L (2013) J Power Sources 236:1–9
18. Lee HW, Muralidharan P, Mari CM, Ruffo R, Kim DK (2011) J Power Sources 196:10712–10716
19. Xiang XD, Fu Z, Li WS (2013) J Solid State Electrochem 17:1201–1206
20. Xiao XC, Lu P, Ahn D (2011) Adv Mater 23:3911–3915
21. Matsuda K, Taniguchi I (2004) J Power Sources 132:156–160
22. Amatucci G, Pasquier AD, Blyr A, Zheng T, Tarascon JM (1999) Electrochim Acta 45:255–271
23. Kim HJ, Choi Y, Yoon S, Cho JJ (2007) Electrochem Commun 9: 801–806
24. Wei GZ, Lu X, Ke FS, Huang L, Li JT, Wang ZX, Zhou ZY, Sun SG (2010) Adv Mater 22:4364–4367
25. Wang J, Yao XY, Zhou XF, Liu ZP (2011) J Mater Chem 21:2544–2549
26. Xiang XD, Li XQ, Li WS (2013) J Power Sources 230:89–95
27. Yi TF, Xie Y, Zhu YR, Ye MF (2012) J Power Sources 211:59–65
28. Talyosef Y, Markovsky B, Salitra G, Aurbach D, Kim HJ, Choi S (2005) J Power Sources 146:664–669
29. Chen D, Li B, Liao Y, Lan H, Lin H, Xing L, Wang Y, Li W (2014) J Solid State Electrochem 18:2027–2033
30. Aklalouch M, Amarilla JM, Saadoune I, Rojo JM (2011) J Power Sources 196:10222–10227
31. Bruce PG, Scrosati B, Tarascon JM (2008) Angew Chem Int Ed Engl 47:2930–2946
32. Wang Y, Li H, He P, Hosono E, Zhou H (2010) Nanoscale 2:1294–1305
33. Li B, Wang YQ, Rong HB, Wang YT, Liu JS, Xing LD, Xu MQ, Li WS (2013) J Mater Chem A 1:12954–12961